

Experimental realization of Dicke states of up to six-qubits for multiparty quantum networking

R. Prevedel¹, G. Cronenberg¹, M. S. Tame², M. Paternostro², P. Walther^{1,3}, M. S. Kim², and A. Zeilinger^{1,3}

¹*Faculty of Physics, University of Vienna, Boltzmannngasse 5, A-1090 Vienna, Austria*

²*School of Mathematics and Physics, The Queen's University, Belfast, BT7 1NN, UK*

³*Institute for Quantum Optics and Quantum Information (IQOQI), Austrian Academy of Sciences, Boltzmannngasse 3, A-1090 Vienna, Austria*

(Dated: October 31, 2021)

We report the first experimental generation and characterization of a six-photon Dicke state. The produced state shows a fidelity of $F = 0.56 \pm 0.02$ with respect to an ideal Dicke state and violates a witness detecting genuine six-qubit entanglement by four standard deviations. We confirm characteristic Dicke properties of our resource and demonstrate its versatility by projecting out four- and five-photon Dicke states, as well as four-photon GHZ and W states. We also show that Dicke states have interesting applications in multiparty quantum networking protocols such as open-destination teleportation, telecloning and quantum secret sharing.

PACS numbers: 03.67.-a, 03.67.Mn, 42.50.Dv, 42.50.Ex, 03.67.Lx

Multipartite entanglement is at the core of studies probing the foundations of quantum physics and represents a key component in a wide range of quantum information processing (QIP) tasks [1]. So far, Greenberger-Horne-Zeilinger (GHZ) [2], W [3], cluster and graph states [4] have been studied and experimentally investigated [5]. However, many other nonequivalent classes of quantum states with interesting and unusual symmetries exist [6]. In particular, Dicke states [7] provide a rich opportunity for exploring multipartite entanglement. Recent studies have focused on techniques for generating, detecting and characterizing these states [8, 9] in atomic, ion-trap [10] and optical [11] settings.

In this Letter we report the experimental generation and investigation of a variety of multi-photon entangled states. We present a flexible linear-optics setup that can produce four-, five- and six-photon representatives of the important class of Dicke states, as well as four-photon GHZ states. Information is encoded in the polarization degrees of freedom of entangled photons produced by high-order spontaneous parametric down conversion (SPDC). We show that our generated states are genuinely multipartite entangled by using tailor-made and experimentally favorable witness tools. These new characterization methods are important in virtue of the non-ideal nature of the six-photon state: although spurious nonlinear processes affect its quality, quantum features can still be observed and characterized. We also highlight the potential for quantum control in large Hilbert spaces by evaluating protocols such as telecloning, open-destination teleportation and quantum secret sharing [11, 12, 13, 14, 15].

Experiment.- Fig. 1 (a) shows the setup for the generation of the three-excitation six-photon Dicke state $|D_6^{(3)}\rangle = \frac{1}{\sqrt{20}} \sum_P |HHHVVV\rangle_{123456}$. Here, $|H/V\rangle_i$ are horizontal/vertical polarization states of a photon in spatial mode $i = 1, \dots, 6$, which encode the logical states of a qubit, while \sum_P denotes the sum over all permutations

of logical states [16]. In the setup, six photons are probabilistically distributed among the spatial modes by non-polarizing beamsplitters (BSs): upon detecting one photon in each mode we post-selectively observe $|D_6^{(3)}\rangle$. We use higher-order emissions of a collinear type-II SPDC process for the simultaneous production of three pairs of photons [17]. A Coherent Inc. Verdi V-18 laser is combined with a mode-locked Mira HP Ti:Sa oscillator to reach the energy necessary to observe *third-order* SPDC emissions. The pulsed-laser output ($\tau = 200$ fs, $\lambda = 810$ nm, 76 MHz) is frequency-doubled using a 2 mm-thick Lithium triborate (LBO) crystal, resulting in UV pulses of 1.4 W cw-average. To avoid optical damage to the anti-reflection coating of the LBO, we continuously translate it with a step-motor, achieving a very stable source of UV pulses (power and count-rate fluctuations less than 1–2% over 30 h). The UV pulses are focused onto a 2 mm-thick β -barium borate (BBO) type-II crystal, cut for collinear down-conversion emission. Dichroic mirrors then separate the down-converted photons from the UV pump and a compensator erases walk-off effects. We use high-transmittivity interference filters ($\Delta\lambda = 3$ nm) to spatially and spectrally select the down-conversion, which is coupled to a single-mode fiber guiding the photons to the *Dicke-setup* of Fig. 1 (a). At 1.4 W of UV pump power, we observe ~ 0.003 six-photon Dicke states per second. Higher power would increase the six-fold rate while decreasing the fidelity due to undesired detection events from higher-order SPDC emissions [17].

State characterization.- In order to detect the presence of genuine multipartite entanglement (GME) in our experimental states, *i.e.* quantum entanglement shared by all the particles involved, we use collective spin inequalities [9]. Various entanglement witnesses have been found to be well-suited to the class of Dicke states [8]. They are experimentally appealing, due to the small number of local measurement settings (LMSs) required, in stark contrast to their more demanding projector-

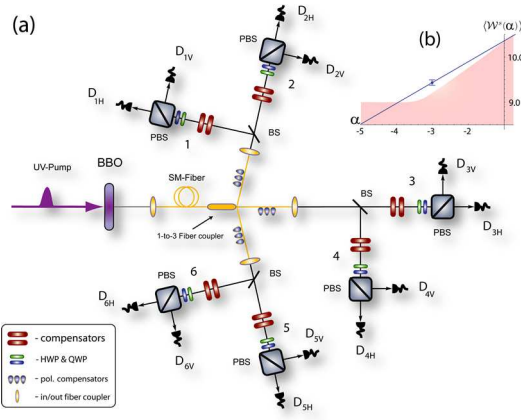


FIG. 1: **(a)**: Setup for the generation of the six-photon Dicke state $|D_6^{(3)}\rangle$. Photons are probabilistically distributed into modes 1, ..., 6 via a 1-to-3 fiber coupler, followed by 50:50 BSs. The expected probability to find one photon in each spatial mode, corresponding to the state $|D_6^{(3)}\rangle$, is $p \sim 0.015$. The fiber and BSs introduce birefringence, compensated by fiber-squeezers and birefringent crystals. State-characterization is performed via polarization-analysis of six-fold coincidences by cascading a quarter-wave plate (QWP), half-wave plate (HWP) and a polarizing beamsplitter (PBS), whose output ports are monitored by multi-mode fiber-coupled single-photon detectors. Each detector signal enters a coincidence logic that records multi-photon coincidences. **(b)**: Biseparability region (shaded) for $\langle \mathcal{W}^s(\alpha) \rangle_{bs}$ and experimental point (predicted line) for $\langle \mathcal{W}^s(\alpha) \rangle_{\rho_6^{(3)}}$.

based counterparts. We start with the collective spin witness $(\mathcal{W}^s)_f = \langle J_x^2 + J_y^2 \rangle_f$, where f refers to the state over which the expectation value is calculated. Here, $J_i = \frac{1}{2} \sum_{k=1}^N \sigma_i^{(k)}$ ($i = x, y, z$) are collective-spin operators of N qubits with label k and $\sigma_i^{(k)}$ denotes the i -Pauli operator. By using the techniques described in Ref. [18], it can be seen that for any six-qubit biseparable (bs) state $\langle \mathcal{W}^s \rangle_{bs} \leq 11.02$, so that $\langle \mathcal{W}^s \rangle_f > 11.02$ will detect the presence of GME in f . However, due to the non-ideal two-qubit correlations upon which \mathcal{W}^s depends (shown in Figs. 2 (a) and (b) for $\langle J_x^2 \rangle$ and $\langle J_y^2 \rangle$), our experimental state $\rho_6^{(3)}$ gives $\langle \mathcal{W}^s \rangle_{\rho_6^{(3)}} < 11.02$. To obtain a witness that detects GME for a non-ideal state, we insert a term proportional to J_z^2 , for which $\langle J_z^2 \rangle_{D_6^{(3)}} = 0$. This gives the more general witness $\mathcal{W}^s(\alpha) = J_x^2 + J_y^2 + \alpha J_z^2$ ($\alpha \in \mathbb{R}$). We then search for values of α such that $\langle \mathcal{W}^s(\alpha) \rangle_{\rho_6^{(3)}} > \langle \mathcal{W}^s(\alpha) \rangle_{bs}$. In Fig. 2 (c) we show the two-qubit correlations for $\langle J_z^2 \rangle_{\rho_6^{(3)}}$, which contribute to $\langle \mathcal{W}^s(\alpha) \rangle$ shown in Fig. 1 (b). A range of α exists where $\langle \mathcal{W}^s(\alpha) \rangle_{\rho_6^{(3)}} > \langle \mathcal{W}^s(\alpha) \rangle_{bs}$: the gap is optimized at $\alpha = -3$, where $\langle \mathcal{W}^s(\alpha) \rangle_{bs}^{\max} - \langle \mathcal{W}^s(\alpha) \rangle_{\rho_6^{(3)}} = -0.24 \pm 0.06$, thus confirming GME for our experimental state.

We now further probe the features of $\rho_6^{(3)}$ and consider the multi-photon correlator $C_{i,j}^{\otimes N}(\theta) = (\cos \theta \sigma_i +$

$\sin \theta \sigma_j)^{\otimes N}$. This allows the sampling of N -photon correlations in orthogonal planes of the single-qubit Bloch sphere, providing important information about the off-diagonal elements of the density matrix and thus its coherence properties. One finds $\langle C_{i,z}^{\otimes 6}(\theta) \rangle_{D_6^{(3)}} = [3 \cos(2\theta) + 5 \cos(6\theta)]/8$, for $i = x, y$. Only the coherences within the Dicke state are responsible for the interference between the trigonometric functions in $\langle C_{i,z}^{\otimes 6}(\theta) \rangle_{D_6^{(3)}}$ [17, 19]. In Figs. 2 (h) and (i) we compare the ideal coherence signature with that of $\rho_6^{(3)}$, finding a reduced visibility. We also compare $\rho_6^{(3)}$ with the behavior of the state ρ_{sim} resulting from a detailed simulation of our setup including multiple-pair emissions and losses [17]. The simulated state spans a Hilbert-space sector which is larger than the 2^6 -dimensional space of $|D_6^{(3)}\rangle$. Moreover, the presence of spurious state-components in ρ_{sim} affects the ideal populations and coherences, as shown in Ref. [17]. The accuracy of the simulation is confirmed by the behavior of $\langle C_{i,j}^{\otimes 6}(\theta) \rangle_{\rho_{sim}}$ shown in Figs. 2 (h) and (i), revealing good agreement with our data. Our analysis of $\rho_6^{(3)}$ is strengthened by evaluating the state fidelity $\langle F_{D_6^{(3)}} \rangle_{\rho_6^{(3)}}$, where the projector $F_{D_6^{(3)}} = |D_6^{(3)}\rangle \langle D_6^{(3)}|$ is decomposed into 544 terms involving Pauli operators, requiring 21 LMSs for their evaluation [20]. We find $\langle F_{D_6^{(3)}} \rangle_{\rho_6^{(3)}} = 0.56 \pm 0.02$, which agrees well with the value 0.61 from ρ_{sim} . The small discrepancy is due to slightly asymmetric fiber-coupling of $|H/V\rangle$ due to SPDC birefringence. The setup performances are thus limited by noise from higher-order emissions [17]. Despite such clearly consistent results, the measured fidelity prevents us from unambiguously claiming that our generated state is Dicke-class [21]. As

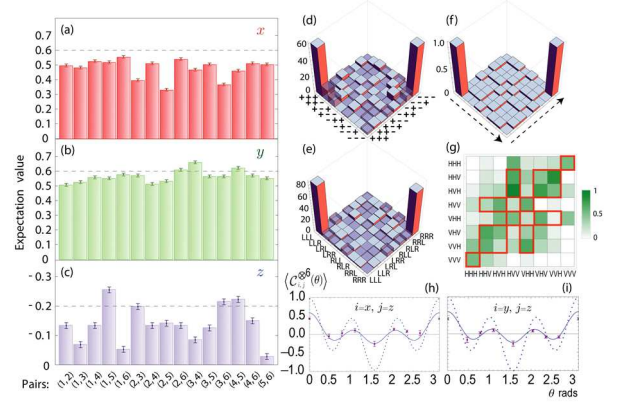


FIG. 2: Experimental study of the six-photon Dicke state $\rho_6^{(3)}$. **(a)-(c)**: Correlations $\langle \sigma_i^{(j)} \sigma_i^{(k)} \rangle$ for qubit pairs (j, k) ($i = x, y, z$) for $\langle \mathcal{W}^s(\alpha) \rangle$. Dashed lines are ideal values. **(d), (e)** and **(g)**: Coincidences for photons measured in $|\pm\rangle = (|H\rangle \pm |V\rangle)/\sqrt{2}$, $|L/R\rangle = (|H\rangle \pm i|V\rangle)/\sqrt{2}$ and $|H/V\rangle$ (rescaled). **(f)**: Ideal populations for **(d)** and **(e)**. **(h)** and **(i)**: Multiphoton correlations. Dashed (solid) lines are the patterns of $\langle C_{x/y,z}^{\otimes 6}(\theta) \rangle$ for $|D_6^{(3)}\rangle$ (ρ_{sim}). The dots are experimental points.

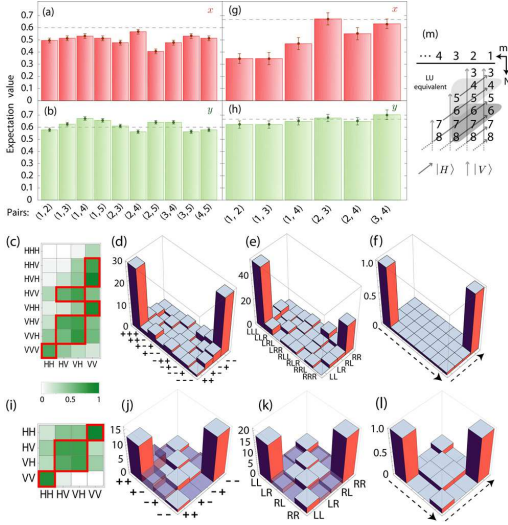


FIG. 3: Experimental data for the Dicke states $\varrho_5^{(2)}$ and $\varrho_4^{(2)}$. (a) and (b) ((g) and (h)): Correlations $\langle \sigma_i^{(j)} \sigma_i^{(k)} \rangle$ for qubit pairs (j, k) of $\varrho_5^{(2)}$ ($\varrho_4^{(2)}$), with $i = x, y$. (c)-(e) ((i)-(k)): Coincidences for the five (four) photons measured in $|H/V\rangle$, $|\pm\rangle$ and $|L/R\rangle$. (f) ((l)): Ideal populations for $|\pm\rangle$ and $|L/R\rangle$. (m): Navigating the Dicke class by measurement.

full state tomography is experimentally prohibitive, we complement the fidelity analysis with additional characterization tools.

We now explore the *nested* structure of Dicke states and their persistence of entanglement by conditionally generating four and five-photon entangled states via projections of $|D_6^{(3)}\rangle$ [11, 22]. For example, by measuring one photon in $|H\rangle$, the five-photon state $|D_5^{(2)}\rangle$ [16] is projected out. This state is equivalent to $\sigma_x^{\otimes 5}|D_5^{(3)}\rangle$, showing that *navigation* through the Dicke class of states is possible via projections and local operations. Indeed, one can write $|D_N^{(m)}\rangle = (C_N^m)^{-1/2}[(C_{N-1}^{m-1})^{1/2}|H\rangle|D_{N-1}^{(m-1)}\rangle + (C_{N-1}^m)^{1/2}|V\rangle|D_{N-1}^{(m)}\rangle]$ and navigate as shown in Fig. 3 (m). We start by experimentally projecting out the five-photon state $\varrho_5^{(2)}$ in modes 2, ..., 6 (Figs. 3 (a)-(f) show the relevant experimental data). For five-qubit states we have $\langle \mathcal{W}^s \rangle_{bs} \leq 7.87$ [18], giving $\langle \mathcal{W}^s \rangle_{bs}^{\max} - \langle \mathcal{W}^s \rangle_{\varrho_5^{(2)}} = -0.21 \pm 0.04$, thus detecting GME (here, $\alpha = 0$ is set due to the good quality of the correlations). To check consistency, we have also projected photon 6 in $|H\rangle$, finding $\langle \mathcal{W}^s \rangle_{bs}^{\max} - \langle \mathcal{W}^s \rangle_{\varrho_5^{(2)}} = -0.32 \pm 0.02$.

Next, we project out the four-photon Dicke state $|D_4^{(2)}\rangle$ [16] by measuring one photon in $|H\rangle$ and another in $|V\rangle$. Using $\langle \mathcal{W}^s \rangle_{bs} \leq 5.23$ [8], the correlations for the experimental state $\varrho_4^{(2)}$ in modes 3, ..., 6 (shown in Figs. 3 (g)-(l)) give $\langle \mathcal{W}^s \rangle_{bs}^{\max} - \langle \mathcal{W}^s \rangle_{\varrho_4^{(2)}} = -0.16 \pm 0.07$, thus detecting GME. Moreover, we have evaluated the state fidelity $\langle F_{D_4^{(2)}} \rangle_{\varrho_4^{(2)}} = 0.66 \pm 0.05$ by implementing the 9-LMS projector $F_{D_4^{(2)}}$ [23]. We complete our

study of four-photon Dicke states by assessing a four-photon W state $|D_4^{(1)}\rangle$ (equivalent to $\sigma_x^{\otimes 4}|D_4^{(3)}\rangle$), generated from $|D_6^{(3)}\rangle$ upon measurement of two photons in $|H\rangle$. Experimentally, we project the state $\varrho_4^{(1)}$ into modes 3, ..., 6 (coincidence counts shown in Figs. 4 (a)-(d)). Although $|D_4^{(1)}\rangle$ does not exceed $\langle \mathcal{W}^s \rangle_{bs}^{\max}$, for our experimental state we find $\langle \mathcal{W}^s \rangle_{bs}^{\max} - \langle \mathcal{W}^s \rangle_{\varrho_4^{(1)}} = -0.2 \pm 0.1$ due to $\langle J_{x,y}^2 \rangle$ being slightly larger than their ideal values, thus detecting GME. We further characterize $\varrho_4^{(1)}$ by evaluating $\langle F_{D_4^{(1)}} \rangle_{\varrho_4^{(1)}} = 0.62 \pm 0.02$, which requires only 7 LMSs [24]. Finally, a state locally equivalent to $|GHZ_4\rangle = (1/\sqrt{2})[|H\rangle^{\otimes 4} + |V\rangle^{\otimes 4}]$ can also be generated from $|D_6^{(3)}\rangle$ by measuring one photon in $|+\rangle$ and another in $|-\rangle$. Ideally, this produces $(|D_4^{(1)}\rangle - |D_4^{(3)}\rangle)/\sqrt{2} \equiv \sigma_z^{(1)}(\mathcal{H}\sqrt{\sigma_z})^{\otimes 4}|GHZ_4\rangle$ (\mathcal{H} is the Hadamard gate). The state fidelity (using 5 LMSs) is $\langle F_{GHZ_4} \rangle_{\varrho_{GHZ}} = 0.56 \pm 0.02$, giving a projector-based witness value of $\langle \mathcal{W} \rangle_{GHZ} = -0.06 \pm 0.02$ [24], thus confirming again GME.

Quantum protocols.- Despite the non-ideal value of the state-fidelity, the symmetries within our six-photon resource make it suitable for several key quantum networking protocols [11, 14], some of which have been demonstrated in four-photon settings. Tracing out $N-2$ qubits, one finds the two-photon state $\rho = \alpha_N|\psi^+\rangle\langle\psi^+| + (1 - \alpha_N)[|HH\rangle\langle HH| + |VV\rangle\langle VV|]/2$ with $\alpha_N = N/[2(N-1)]$ for $N \geq 4$ [9] and $|\psi^\pm\rangle = (|HV\rangle \pm |VH\rangle)/\sqrt{2}$. Here, the maximal singlet fraction F_{msf} [25], given by the maximum of $\langle F_{\psi^-} \rangle$ under local operations and classical communication, helps in assessing the usefulness of ρ for networking tasks. We consider using ρ as a teleportation channel [11, 14], where the maximum fidelity achievable for teleporting an arbitrary state is $F_{\text{max}} = (2F_{\text{msf}} + 1)/3$. For $|D_N^{(N/2)}\rangle$, $F_{\text{msf}} = \alpha_N$, thus $F_{\text{max}} = \frac{2N-1}{3(N-1)}$. Fig. 4 (e) shows F_{max} for all pairs of photons from $\varrho_6^{(3)}$ and the ideal value 0.73 (upper dashed-line). As any photon pair in $|D_6^{(3)}\rangle$ provides a channel for teleportation, regardless of operations applied to the others, one can use it for telecloning [11, 12, 13]. The fidelity-limit for universal symmetric $1 \rightarrow (N-1)$ cloning is exactly F_{max} [13], thus $|D_N^{(N/2)}\rangle$ is an ideal resource for this task. Following [12], we have evaluated the protocol using $\varrho_6^{(3)}$: Fig. 4 (e) shows that the maximum cloning fidelity achievable is consistently above the classical threshold of $2/3$ [13]. A perfect $|\psi^+\rangle$ channel for teleportation can be created, with success probability α_N , if $N-2$ photons are *measured* out of $|D_N^{(N/2)}\rangle$ in the $|H/V\rangle$ basis. This is in contrast to telecloning, where the photons are traced-out, resulting in an imperfect channel with fidelity $\langle F_{\psi^+} \rangle_\rho = \alpha_N$. As the core operation needed for telecloning commutes with the $|H/V\rangle$ measurements, one can choose between telecloning and teleportation [11], with the success probability to teleport to any one party

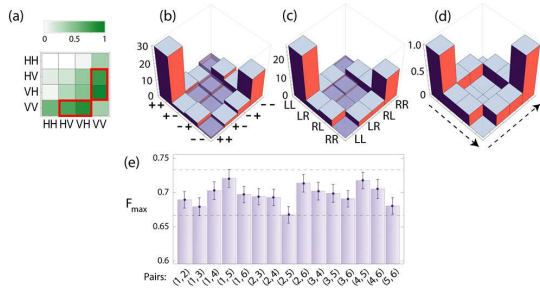


FIG. 4: Experimental data for the W-state $\varrho_4^{(1)}$. **(a)-(c)**: Coincidence counts for $\varrho_4^{(1)}$ in the rescaled $|H/V\rangle$, $|\pm\rangle$ and $|L/R\rangle$ bases. **(d)**: Ideal populations for **(b)** and **(c)**. **(e)**: Maximum achievable fidelity F_{\max} using pair (i, j) as a channel. The upper (lower) line shows the ideal (classical) value.

given by $p_s = \alpha_N \geq \frac{1}{2}$. Thus $|D_6^{(3)}\rangle$ can be used for open destination teleportation [11, 14]. For $\varrho_6^{(3)}$ we find a mean value $\bar{p}_s = 0.55 \pm 0.02$ very close to the ideal $p_s = 0.6$. As an example, we choose photons 5 and 6, finding a mean fidelity $\langle \bar{F}_{\psi^+} \rangle_{\rho_{exp}} = 0.71 \pm 0.02$.

Finally, $|D_N^{(N/2)}\rangle$ can also be used for multiparty quantum secret sharing [15], where entanglement ensures that all parties must cooperate in order to obtain a shared secret. The trick is to exploit the perfect correlations in the maximally-conjugate bases of $\sigma_{x,y}$. Using $\langle C_{i,j}^{\otimes N}(\theta) \rangle$, we get $\langle \sigma_{x,y}^{\otimes N} \rangle_{D_N^{(N/2)}} = 1$. Consider the σ_x basis and $x_j \in \{0, 1\}$ as the measurement-outcome for the j -th photon. If photon 1 is measured, the value of x_1 can only be recovered via $x_1 = \oplus_{i=2}^N x_i$ (\oplus denotes mod-2 addition), implying cooperation of parties 2, ..., N . As $|D_N^{(N/2)}\rangle$ is symmetric, this applies to any choice for the initial party. The same holds for the σ_y basis. When the parties announce their (randomly chosen) bases, a shared-key can be distributed [15], with which a designated party encodes the secret. Any set of less than $N-1$ parties cannot recover the key and although subsets of parties can exist with partial information about x_1 (for instance), any such bias is removable by post-processing [15, 26]. We thus evaluated the expected quantum bit error-rate of the generated key (before post-processing), given by the average error rate of the $\sigma_{x,y}$ bases. We find $25 \pm 2\%$ and $29 \pm 1\%$ for $N = 4$ (415 shared bits) and $N = 6$ (889 shared bits) respectively over an 82 hour period.

Remarks.- We have demonstrated a linear-optics setup able to produce various states from the Dicke class and characterized their properties using new methods. We also evaluated the potential of our six-photon state for multiparty quantum networking. Our work significantly extends the range of attainable quantum states and paves the way toward the experimental study of other six-qubit entangled states [6] (and larger ones) and their use in QIP.

Acknowledgments.- We acknowledge discussions with J. Kofler, T. Jennewein and N. Langford, help from B. Rauer and support from EPSRC, QIPIRC, FWF, EC

under the Integrated Project Qubit Application, EMALI and the U.S. Army Research Funded IARPA.

-
- [1] R. Horodecki, *et al.*, Rev. Mod. Phys. **81**, 865 (2009).
 - [2] D.M. Greenberger, *et al.*, Am. J. Phys. **58**, 1131 (1990).
 - [3] W. Dür, G. Vidal, and J.I. Cirac, Phys. Rev. A **62**, 062314 (2000).
 - [4] H.J. Briegel *et al.* Nature Phys. **5**, 19 (2009).
 - [5] D. Bouwmeester *et al.*, Phys. Rev. Lett., **82**, 1345 (1999); M. Eibl *et al.*, *ibid.*, **90**, 200403 (2003); Z. Zhao *et al.*, Nature (London), **430**, 54 (2004); H. Häffner *et al.*, *ibid.* **438**, 643 (2005); C.-Y. Lu *et al.*, Nature Phys. **3**, 91 (2007); W. Wieczorek *et al.*, Phys. Rev. Lett. **101**, 010503 (2008); W.-B. Gao *et al.*, arXiv:0809.4277 (2008);
 - [6] F. Verstraete, *et al.*, Phys. Rev. A **65**, 052112 (2002); L. Chen and Y. Chen, *ibid.* **74**, 062310 (2006); L. Lamata, *et al.*, *ibid.* **75**, 022318 (2007).
 - [7] R.H. Dicke, Phys. Rev. **93**, 99 (1954).
 - [8] G. Tóth, J. Opt. Soc. Am. B **24**, 275 (2007).
 - [9] A. Sørensen, *et al.*, Nature (London) **409**, 63 (2001); J.K. Stockton, *et al.*, Phys. Rev. A **67**, 022112 (2003); J. Korbicz, J.I. Cirac and M. Lewenstein, Phys. Rev. Lett. **95**, 120502 (2005); G. Tóth, *et al.*, *ibid.* **99**, 250405 (2007); J. Korbicz, *et al.*, Phys. Rev. A **74**, 052319 (2006).
 - [10] C. Thiel *et al.*, Phys. Rev. Lett. **99**, 193602 (2007); J.K. Stockton, R. van Handel and H. Mabuchi, Phys. Rev. A **70**, 022106 (2004); A. Retzker, E. Solano and B. Reznik, *ibid.* **75**, 022312 (2007); I.E. Linington and N.V. Vitanov, *ibid.* **77**, 010302(R) (2008).
 - [11] N. Kiesel *et al.*, Phys. Rev. Lett. **98**, 063604 (2007).
 - [12] M. Muraio, *et al.*, Phys. Rev. A **59**, 156 (1999).
 - [13] V. Scarani, *et al.*, Rev. Mod. Phys. **77**, 1225 (2005).
 - [14] C.H. Bennett *et al.*, Phys. Rev. Lett. **70**, 1895 (1993); A. Karlsson and M. Bourennane, Phys. Rev. A **58**, 4394 (1998).
 - [15] M. Hillery, V. Bužek and A. Berthiaume, Phys. Rev. A **59**, 1829 (1999).
 - [16] A Dicke state of N qubits and k excitations is given by $|D_N^{(k)}\rangle = (C_N^k)^{-1/2} \sum_P |H\rangle^{\otimes k} |V\rangle^{\otimes N-k}$, with C_i^j as the binomial coefficient.
 - [17] See EPAPS Document No. E-PRLTAO-103-082929. For more information on EPAPS, see <http://www.aip.org/pubservs/epaps.html>.
 - [18] S. Campbell, M. S. Tame and M. Paternostro, arXiv:0903.3939v1, to appear in New J. Phys. (2009).
 - [19] A dephasing mechanism affecting $|D_6^{(3)}\rangle$ leads to the single term $(\sin \theta)^6$ [18].
 - [20] The LMSs are $\sigma_{x,y,z}^{\otimes 6}$, $[(\sigma_x \pm \sigma_{y,z})/\sqrt{2}]^{\otimes 6}$, $[(\sigma_y \pm \sigma_z)/\sqrt{2}]^{\otimes 6}$, $[(\sigma_{x,y} \pm 2\sigma_z)/\sqrt{5}]^{\otimes 6}$, $[(\sigma_z \pm 2\sigma_{x,y})/\sqrt{5}]^{\otimes 6}$ and $[(\sigma_x \pm \sigma_y \pm \sigma_z)/\sqrt{3}]^{\otimes 6}$.
 - [21] In the $\sigma_{x,y}$ bases, for instance, $|D_6^{(3)}\rangle$ has an overlap of $\sqrt{5/8}$ with a six-photon GHZ state.
 - [22] This was independently investigated in W. Wieczorek *et al.*, Phys. Rev. A **79**, 022311, (2009).
 - [23] The LMSs are $\sigma_{x,y,z}^{\otimes 4}$, $[(\sigma_x \pm \sigma_{y,z})/\sqrt{2}]^{\otimes 4}$, $[(\sigma_y \pm \sigma_z)/\sqrt{2}]^{\otimes 4}$.
 - [24] O. Gühne, *et al.*, Phys. Rev. A **76**, 030305(R) (2007).
 - [25] M. Horodecki, P. Horodecki and R. Horodecki, Phys. Rev. A **60**, 1888 (1999).
 - [26] S. Gaertner, *et al.*, Phys. Rev. Lett. **98**, 020503 (2007).